IEEE Access
Multidisciplinary | Rapid Review | Open Access Journal

Received 10 April 2023, accepted 2 May 2023, date of publication 8 May 2023, date of current version 11 May 2023.

Digital Object Identifier 10.1109/ACCESS.2023.3273779

RESEARCH ARTICLE

Computation of 3-D Electric Field on Buildings of Arbitrary Shape Near HVDC Transmission Lines

PO LONG[1], GUOCAI ZUO[2], KUN HE[3], AND LI XIE[3]

[1]Software College, Changsha Social Work College, Changsha 410004, China
[2]School of Software and Information Engineering, Hunan Software Vocational and Technical University, Xiangtan 411100, China
[3]Tibet Yangbajing High Altitude Electrical Safety and Electromagnetic Environment National Observation and Research Station, China Electric Power Research Institute, Beijing 100192, China

Corresponding authors: Po Long (longpo@csmzxy.edu.cn), Guocai Zuo (zuoguocai@hnsoftedu.com), and Kun He (kh880622@126.com)

This work was supported in part by the State Grid Corporation of China under Grant 5200-202255084A-1-1-ZN, and in part by the 2022 Annual Project of the 14th Five Year Plan for Educational Science in Hunan Province under Grant XJK22CXX005.

ABSTRACT Electrical environment of residences adjacent to Ultra high voltage direct current (UHVDC) transmission lines draws huge attentions as it affects people's lives. Predicting electric field is a crucial part during the design and environmental impact assessments of HVDC transmission lines. However, traditional methods have difficulty coping with the complex geometry of residences and bundled line conductors simultaneously. To deal with this issue, a line-area element hybrid boundary element method is proposed, combined with flux tracing method, to compute 3D total electric field on buildings of arbitrary shape near HVDC transmission lines. Line and area elements are used to discretize bundled line conductors and buildings, respectively. Its correctness is validated by the experimental data reported in the literature, with a maximum relative error of about 10 % on the top of residences. Its applicability is demonstrated by several case studies encountered in practical UHVDC transmission projects. The results also show that parapet walls can weaken the electric field on platforms of residences. In the case presented in this paper, the TEF is reduced by about 58 %. This work can provide theoretical and technical support for the design and environmental impact assessments of HVDC transmission lines.

INDEX TERMS HVDC transmission, electrical environment, adjacent residences, complex geometrical shape, total electric field, boundary element method, flux tracing method.

I. INTRODUCTION

To achieve the goal of carbon emission peak and carbon neutrality, China is putting a huge effort into constructing renewable energy production bases and ultra-high voltage direct current (UHVDC) transmission projects. The UHVDC transmission overhead lines pass through several thousand kilometers transmitting energy from the bases to the loads. Attention has been drawn to the electrical environment of residences adjacent to the lines, especially after the issue of the Chinese National Standard GB39220-2020 [1] which for the first time sets limit values for electric fields on balconies and platforms where human activities take place. Before the publishing of the standard, by HVDC transmission line design norms, it was common practice to merely assume the residences were not present and require the electric field on the location of residences not to exceed 25 kV/m. Now the effects of residences on the field have to be taken into account and the fields on balconies and platforms of residences have become the decisive factor impacting line heights, which influences construction costs considerably. This problem is faced by all UHVDC transmission projects under planning or construction in China.

Due to the presence of ion flows generated by corona discharges in the vicinity of HVDC lines, the electric field is composed of two parts: the space-charge-free one produced by the applied voltage and the space-charge one stimulated by the moving ions. To differentiate this field from the static electric field, it is termed the **total electric field** (**TEF**) [2]. There are mainly four types of methods for

The associate editor coordinating the review of this manuscript and approving it for publication was Mahdi Pourakbari Kasmaei.

computing TEF. They are flux tracing method (FTM), method of characteristics (MOC) upstream finite element method (UFEM) and finite difference method (FDM). The former three have been applied to the prediction of TEF on residences of cubic shape adjacent to HVDC lines. Zhen et al. [3] extended the 2D UFEM for HVDC lines to residences near lines. Later, they proposed a 2D/3D UFEM to cope with issues of heavy memory usage and time consumption brought by fully 3D UFEM [4]. A virtual box is set to enclose the house, and outside the box the 2D UFEM is used to determine the boundary conditions, while inside the box the 3D UFEM is employed to calculate the TFF. Wang et al. proposed a data-driven 3D TEF reconstruction method to correct the 2D calculation results [5]. Luo et al. applied the 2D FTM to calculate the TEF under HVDC lines with buildings nearby [6]. Later they extended this method into a 3D one and computed the 3D TEF distribution on buildings [7]. To accelerate the iteration process, Ma et al. put forward an adaptive iteration strategy [2] With respect to MOC, Xiao et al. first introduced a hybrid 2D/3D MOC to compute TEF near a metal board house under the HVDC line [8]. Xiao et al. improved the iterative process in the 3D MOC and applied the 3D MOC to the calculation of TEF on metal building surfaces [9]. Recently, FDM has been extended to calculate TEF around HVDC conductors Qiao et al. combined FDM with FEM to solve the bipolar ion flow field with strong wind [10] Liu et al. proposed a finite-difference relaxation (FDR) method to achieve massively parallel computation [11] Abouelatta et al. employed the multigrid method as a iterative solver for the FDM in resolving the unipolar corona phenomenon with fine meshes to reduce computational time [12], [13], [14], [15]

UFEM and MOC are difficult to handle in practical cases with bundle conductors because meshing long bundle conductors with a fine radius in 3D cases leads to a huge number of mesh elements, which is computationally demanding. Additionally, they require meshing the entire computational domain. While FTM does not have these demerits due to its use of the charge simulation method (CSM) for the space-charge-free electric field Its effectiveness for buildings of cubic shape has been proven by both indoor reduced-scale and outdoor full-scale experiments [5], [7]. Furthermore, FTM is currently the fastest of the three methods for 3D computations mainly due to its mesh-free feature and it merely needs to compute TEF in the targeted local regions. However, up to this point, all three methods can only be applied to cases where residences have simple shapes, such as a cube. While in practice, houses near HVDC lines are of complex appearances that the forgoing methods are difficult to apply. Complex geometry leads to a greater number of volumetric mesh elements in UFEM and MOC. While in FTM, line segment charges and point charges are placed beneath the line sub-conductor surfaces and house surfaces, respectively. Complex geometry results in an increased number of point charges, which leads to heavy memory usage and large time consumption for FTM. More importantly, it is hard to generate point charges when dealing with residences with complex shapes

Since FTM is mesh-free and able to handle bundle conductors, it is employed in this paper. To resolve the issue of complex geometry in CSM, a line-area element hybrid boundary element method (BEM) is proposed to compute the space-charge-free electric field which can then be used to compute TEF by FTM. In comparison with CSM, it has several advantages. It can handle arbitrary complex geometries with fewer degrees of freedom by incorporating area element for residences and line segment element for bundle conductors. It can directly obtain the surface charge densities and therefore electric fields on sub-conductor surfaces which are required in FTM. Moreover, it eliminates the laborious task of determining the location and number of charges that is required in CSM.

The contribution of this paper is mainly two-fold:

(1) A line-area element hybrid boundary element method (BEM) is proposed to compute the space-charge-free electric field in FTM, thereby addressing the issues related to bundle conductors and residences of complex geometry.

(2) TEFs on residences of complex geometry adjacent to full-scale UHVDC transmission lines are computed and analyzed.

II. PROBLEM DESCRIPTION

When a HVDC transmission line is in operation, the electric field on the line conductor surface is so intense that air ionization takes place near the line. However, due to the sharp drop of electric field at a distance from line, ionization can only occur in a narrow space limited to the line conductor surface. This ionization is called corona discharge. Once the discharge happens, ions are generated and drift towards the ground and the line conductors of the opposite polarity under the action of the electric field [16]. For HVDC corona, the ions will eventually move into the conductors with opposite polarity or towards the ground or infinity, since the direction of the electric field cannot change back and forth as in the case of high voltage alternating current (HVAC) corona. Meanwhile, ions are space charges that can stimulate electric fields and thus distort the space-charge-free electric field. In this way, corona ions and electric fields are tightly coupled. The electric field including the contribution coming from moving corona ions is called total electric field (TEF). In the presence of residences near the lines, TEF shall be distorted at their locations. A sketch of a residence near an HVDC transmission line is displayed in Figure 1.

The mathematical model describing TEF distribution around a bipolar HVDC transmission line can be formulated as [2]

$$\nabla^2\varphi = -\left(\rho_+ - \rho_-\right)/\varepsilon_0 \tag{1}$$

$$\begin{cases} \nabla\cdot\left(\rho_+ k_+ \boldsymbol{E}_\mathrm{s}\right) = -R_\mathrm{i}\rho_+\rho_-/e \\ \nabla\cdot\left(\rho_- k_- \boldsymbol{E}_\mathrm{s}\right) = R_\mathrm{i}\rho_+\rho_-/e \end{cases} \tag{2}$$

$$\boldsymbol{E}_\mathrm{s} = -\nabla\varphi \tag{3}$$

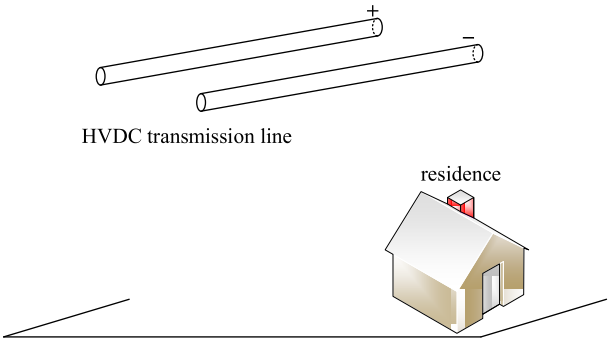

FIGURE 1. A HVDC transmission line with a nearby residence.

where φ is the potential; ρ_+ and ρ_- are the positive and negative charge density, respectively; ε_0 is the permittivity of air; $\boldsymbol{E}_\mathrm{s}$ is the TEF; k_+ and k_- are the positive and negative ion mobility, respectively;R_i is the ion recombination coefficient; e is the elementary charge. On the conductor surfaces, the ground and the residence, potentials for (1) are known. Kaptzov's condition, which states the electric fields on the conductor surfaces remain the corona onset field, is used as a boundary condition for (2). Accordingly, the boundary conditions are

$$\varphi|_{\Gamma 1} = V \tag{4}$$
$$\varphi|_{\Gamma 2} = 0 \tag{5}$$
$$\partial\varphi/\partial n|_{\Gamma 1} = E_\mathrm{on} \tag{6}$$

where V is the voltage applied onto line conductors, E_on is the corona onset electric field, Γ_1 are the line surfaces, Γ_2 are the ground and residence surfaces.

III. BOUNDARY ELEMENT METHOD WITH HYBRID LINE-AREA ELEMENTS

A. METHOD DESCRIPTION

To solve the above-mentioned mathematical model, FTM is adopted in which Deutsch assumption plays a key role. It stipulates that the space charge carried by corona ions changes the magnitude of the electric field without distorting the direction of TEF. By this assumption,

$$\boldsymbol{E}_\mathbf{s} = A\boldsymbol{E} \tag{7}$$

where $\boldsymbol{E}$ is the space-charge-free electric field and A is a scalar and space dependent. As a result, the calculation of the space-charge-free electric field $\boldsymbol{E}$ is the cornerstone of FTM. In this paper, the boundary element method is introduced into FTM for the first time to compute $\boldsymbol{E}$. Conventionally, area elements such as planar triangular elements are employed to discretize the whole geometry. However, it leads to huge amount of elements when line conductors are present. To cope with this issue, line element and area element are proposed to discretize the line conductors and residences, respectively. For line conductors of radius r, assuming the charge is concentrated at the axis of the conductor and its density is τ, the potential φ_l stimulated by the line charge l is given by

$$\varphi_l = \int_l \left(\frac{1}{4\pi\varepsilon_0 R_l} - \frac{1}{4\pi\varepsilon_0 R_{l'}}\right)\tau\, dl \tag{8}$$

where R_l is distance between the line charge and the field point, $R_{l'}$ is the distance between the image of the line charge relative to the ground and the field point. For residence, the potential φ_l stimulated by the surface charge S with charge density σ is given by

$$\varphi_S = \int_S \left(\frac{1}{4\pi\varepsilon_0 R_S} - \frac{1}{4\pi\varepsilon_0 R_{S'}}\right)\sigma\, dS \tag{9}$$

where R_S is distance between the surface charge and the field point, $R_{S'}$ is the distance between the image of the surface charge relative to the ground and the field point. The potential φ generated by the line and the residence is thus given by

$$\begin{aligned}\varphi &= \varphi_l + \varphi_S \\ &= \int_l \left(\frac{1}{4\pi\varepsilon_0 R_l} - \frac{1}{4\pi\varepsilon_0 R_{l'}}\right)\tau\, dl \\ &\quad + \int_S \left(\frac{1}{4\pi\varepsilon_0 R_S} - \frac{1}{4\pi\varepsilon_0 R_{S'}}\right)\sigma\, dS\end{aligned} \tag{10}$$

Linear interpolation functions N_l and N_S are used to reconstruct the charge densities τ and σ, respectively. The potential φ is discretized by Galerkin weighted residual method. For field elements on line conductors, the discretization is formulated as

$$\begin{aligned}&\sum_{elf}\sum_{j}\sum_{i}\int_{lf} N_{lj}N_{li}\varphi_i dlf \\ &= \sum_{elf}\sum_{els}\sum_{j}\sum_{i}\int_{lf} N_{lj} \\ &\quad \times \int_{ls}\left(\frac{1}{4\pi\varepsilon_0 R_l} - \frac{1}{4\pi\varepsilon_0 R_{l'}}\right)N_{li}\tau_i dlsdlf \\ &\quad + \sum_{elf}\sum_{eSs}\sum_{j}\sum_{i}\int_{lf} N_{lj} \\ &\quad \times \int_{Ss}\left(\frac{1}{4\pi\varepsilon_0 R_S} - \frac{1}{4\pi\ \varepsilon_0 R_{S'}}\right)N_{Si}\sigma_i dSsdlf\end{aligned} \tag{11}$$

$$\begin{aligned}&\sum_{eSf}\sum_{j}\sum_{i}\int_{Sf} N_{Sj}N_{li}\varphi_i dSf \\ &= \sum_{eSf}\sum_{els}\sum_{j}\sum_{i}\int_{Sf} N_{Sj} \\ &\quad \times \int_{ls}\left(\frac{1}{4\pi\varepsilon_0 R_l} - \frac{1}{4\pi\varepsilon_0 R_{l'}}\right)N_{li}\tau_i dlsdSf \\ &\quad + \sum_{eSf}\sum_{eSs}\sum_{j}\sum_{i}\int_{Sf} N_{Sj} \\ &\quad \times \int_{Ss}\left(\frac{1}{4\pi\varepsilon_0 R_S} - \frac{1}{4\pi\ \varepsilon_0 R_{S'}}\right)N_{Si}\sigma_i dSsdSf\end{aligned} \tag{12}$$

where *elf*, *els*, *eSf* and *eSs* are field line element, source line element, field area element and source area element, respectively. *lf*, *ls*, *Sf* and *Ss* are integration domain on field line element, integration domain on source line element, integration domain on field area element and integration domain on source area element, respectively. The subscripts i and j denote the ith and jth elements. For field elements on residences, the discretization is formulated as

$$\begin{aligned}
&\sum_{elf}\sum_{j}\sum_{i}\int_{lf} N_{lj}N_{Si}\varphi_i dlf \\
&= \sum_{elf}\sum_{els}\sum_{j}\sum_{i}\int_{lf} N_{lj} \\
&\quad \times \int_{ls}\left(\frac{1}{4\pi\varepsilon_0 R_l}-\frac{1}{4\pi\varepsilon_0 R_{l'}}\right)N_{li}\tau_i dlsdlf \\
&\quad + \sum_{elf}\sum_{eSs}\sum_{j}\sum_{i}\int_{lf} N_{lj} \\
&\quad \times \int_{Ss}\left(\frac{1}{4\pi\varepsilon_0 R_S}-\frac{1}{4\pi\ \varepsilon_0 R_{S'}}\right)N_{Si}\sigma_i dSsdlf \qquad (13)
\end{aligned}$$

$$\begin{aligned}
&\sum_{eSf}\sum_{j}\sum_{i}\int_{Sf} N_{Sj}N_{Si}\varphi_i dSf \\
&= \sum_{eSf}\sum_{els}\sum_{j}\sum_{i}\int_{Sf} N_{Sj} \\
&\quad \times \int_{ls}\left(\frac{1}{4\pi\varepsilon_0 R_l}-\frac{1}{4\pi\varepsilon_0 R_{l'}}\right)N_{li}\tau_i dlsdSf \\
&\quad + \sum_{eSf}\sum_{eSs}\sum_{j}\sum_{i}\int_{Sf} N_{Sj} \\
&\quad \times \int_{Ss}\left(\frac{1}{4\pi\varepsilon_0 R_S}-\frac{1}{4\pi\ \varepsilon_0 R_{S'}}\right)N_{Si}\sigma_i dSsdSf \qquad (14)
\end{aligned}$$

The foregoing equations lead to a system of linear algebraic equations in the form of matrix

$$\boldsymbol{C\lambda} = \boldsymbol{P\varphi} \qquad (15)$$

where

$$\boldsymbol{C} = [C_{ij}] = \begin{bmatrix} C_{i1,j1} \\ C_{i2,j2} \\ C_{i3,j3} \\ C_{i4,j4} \end{bmatrix} \qquad (16)$$

$$\begin{aligned}
C_{i1,j1} &= \sum_{elf}\sum_{els}\int_{lf} N_{lj1}\int_{ls}\left(\frac{1}{4\pi\varepsilon_0 R_l}-\frac{1}{4\pi\varepsilon_0 R_{l'}}\right)N_{li1}dlsdlf \\
&\quad + \sum_{elf}\sum_{eSs}\int_{lf} N_{lj1}\int_{Ss}\left(\frac{1}{4\pi\varepsilon_0 R_S}-\frac{1}{4\pi\varepsilon_0 R_{S'}}\right)N_{Si1}\sigma_{i1}dSsdlf
\end{aligned}$$

$$\begin{aligned}
C_{i2,j2} &= \sum_{eSf}\sum_{els}\int_{Sf} N_{Sj2}\int_{ls}\left(\frac{1}{4\pi\varepsilon_0 R_l}-\frac{1}{4\pi\varepsilon_0 R_{l'}}\right)N_{li2}dlsdSf \\
&\quad + \sum_{eSf}\sum_{eSs}\int_{Sf} N_{Sj2}\int_{Ss}\left(\frac{1}{4\pi\varepsilon_0 R_S}-\frac{1}{4\pi\varepsilon_0 R_{S'}}\right)N_{Si2}dSsdSf
\end{aligned}$$

$$\begin{aligned}
C_{i3,j3} &= \sum_{elf}\sum_{els}\int_{lf} N_{lj3}\int_{ls}\left(\frac{1}{4\pi\varepsilon_0 R_l}-\frac{1}{4\pi\varepsilon_0 R_{l'}}\right)N_{li3}dlsdlf \\
&\quad + \sum_{elf}\sum_{eSs}\int_{lf} N_{lj3}\int_{Ss}\left(\frac{1}{4\pi\varepsilon_0 R_S}-\frac{1}{4\pi\varepsilon_0 R_{S'}}\right)N_{Si3}dSsdlf
\end{aligned}$$

$$\begin{aligned}
C_{i4,j4} &= \sum_{eSf}\sum_{els}\int_{Sf} N_{Sj4}\int_{ls}\left(\frac{1}{4\pi\varepsilon_0 R_l}-\frac{1}{4\pi\varepsilon_0 R_{l'}}\right)N_{li4}dlsdSf \\
&\quad + \sum_{eSf}\sum_{eSs}\int_{Sf} N_{Sj4}\int_{Ss}\left(\frac{1}{4\pi\varepsilon_0 R_S}-\frac{1}{4\pi\varepsilon_0 R_{S'}}\right)N_{Si4}dSsdSf
\end{aligned}$$

$$\boldsymbol{P} = [P_{ij}] = \begin{bmatrix} P_{i1,j1} \\ P_{i2,j2} \\ P_{i3,j3} \\ P_{i4,j4} \end{bmatrix} \qquad (17)$$

$$P_{i1,j1} = \sum_{elf}\int_{lf} N_{lj1}N_{Si1}dlf$$

$$P_{i2,j2} = \sum_{eSf}\int_{Sf} N_{Sj2}N_{li2}dSf$$

$$P_{i3,j3} = \sum_{elf}\int_{lf} N_{lj3}N_{Si3}dlf$$

$$P_{i4,j4} = \sum_{eSf}\int_{Sf} N_{Sj4}N_{Si4}dSf$$

$$\boldsymbol{\lambda} = \begin{bmatrix} \tau_i & \sigma_i \end{bmatrix}^T \qquad (18)$$

$$\boldsymbol{\varphi} = [\varphi_i]^T \qquad (19)$$

where subscripts $i_1, i_2, i_3, i_4, j_1, j_2, j_3, j_4$ are integers, $\boldsymbol{C}$ is the potential coefficient matrix, $\boldsymbol{P}$ is the coefficient vector, λ is a vector containing line charge density τ and surface charge density σ, and $\boldsymbol{\varphi}$ is the potential vector Once charge densities on line conductors and residences are calculated, the space-charge-free electric field $\boldsymbol{E}$ on them are also determined by

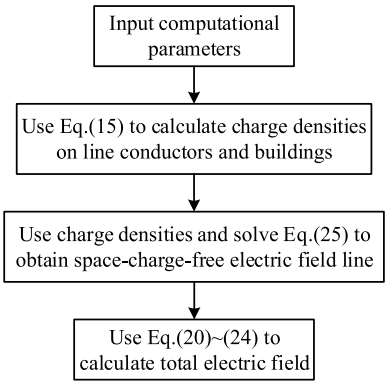

FIGURE 2. The computation flowchart of the proposed method.

$E = \tau/(2\pi r\varepsilon)$. Along the electric field line, one can compute the TEF by the following set of equations [7]

$$A\rho = A_e\rho_e \tag{20}$$

$$\frac{1}{\rho^2} = \frac{1}{\rho_e^2} + \frac{2}{\varepsilon_0 A_e \rho_e}\int_{\varphi_1}^{V} E^{-2}d\varphi \tag{21}$$

$$\rho_m = \frac{\int_0^V \int_\varphi^V E^{-2}\rho d\eta d\varphi}{\int_0^V \int_\varphi^V E^{-2} d\eta d\varphi} \tag{22}$$

$$\rho_m = \frac{\varepsilon_0 (V - V_0)}{\int_0^V \int_\varphi^V E^{-2} d\eta d\varphi} \tag{23}$$

$$A^2 = A_e^2 + \frac{2A_e\rho_e}{\varepsilon_0}\int_{\varphi_1}^{V} E^{-2}d\varphi \tag{24}$$

where ρ_e and A_e are the space charge density ρ and the value of A on line conductor surfaces, respectively, V is the corona onset voltage, V is the applied voltage, φ_1 is the potential at arbitrary point in the space η is the integral variable, and ρ_m is the mean space charge density. It should be noted that A_e can be determined by equation (7). BEM can directly give $\boldsymbol{E}$ on line conductor surfaces and accordingly A_e, while CSM is not able to.

As can be seen from the above equations, one has to determine the electric field lines before calculating TEF. This is achievable by solving the following ordinary differential equations

$$\frac{dx}{E_x} = \frac{dy}{E_y} = \frac{dz}{E_z} \tag{25}$$

where dx, dy, dz are the differentials; E_x, E_y, E_z are the three components of $\boldsymbol{E}$ in Cartesian coordinate system The space-charge-free electric field $\boldsymbol{E} = (E_x, E_y, E_z)$ is computable by virtue of the foregoing proposed boundary element method with line-area hybrid element. The detail of determining the electric field lines can be found in [7].

B. ALGORITHM DESCRIPTION

The workflow of the proposed method is displayed in Figure 2. The computational parameters including line conductor parameters, building parameters and other parameters, such as the relative position between the line and the building. Once these parameters are given, the charge densities on line conductors and buildings can be calculated by virtue of the proposed line-area element hybrid boundary element method. With the help of the charge densities and equation (25), the space-charge-free electric field lines are computable. Thereafter, the TEF can be determined by solving equation(20)~(24).

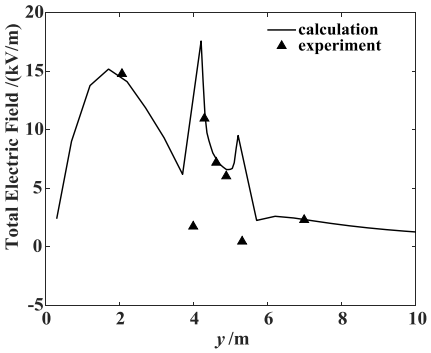

FIGURE 3. Verification of proposed method under a reduced-scale HVDC test line near a reduced-scale residence.

IV. VALIDATION OF THE METHOD

In this section, the proposed method is validated by experimental results reported in [5] and [7]. In [7], the diameter of the line conductor is 13.61 mm, the line height is 2.1 m, the separation between the bipolar conductors is 2.2 m and the applied voltage is ±100 kV. The residence model is 0.5 m in height, 1m in width and 2m in length, and it is 4m away from the line center. The computational and experimental results are presented in Figure 3. In practice, TEFs on the top of residences and under the lines are of primary concern. The maximum relative error on the top of the reduced-scale residence is about 10 % and that under the line is about 2%. It can be seen that the computational result is in good agreement with the experimental result.

In [5], the conductor is six-split bundled with a spacing of 45 cm, the diameter of each sub-conductor is 36.23 mm, the line height is 19 m, and separation between the bipolar conductors is 22 m and the applied voltage is ±800 kV. The residence model is 4m in height, 6m in width and 12 m in length, and it is 30 m away from the line center. The computational and experimental results are presented in Figure 4. In practice, TEFs on the top of residences and under the lines are of primary concern. The maximum relative error on the top of the full-scale residence where TEF is concerned is about 3 % and that under the line is about 10 %. It can be seen that the computational result is in good agreement with the experimental result. In summary, the correctness of the proposed method is verified.

V. PRACTICAL CASE STUDIES AND DISCUSSIONS

In this section, the proposed method is applied to several practical cases encountered during the design of the

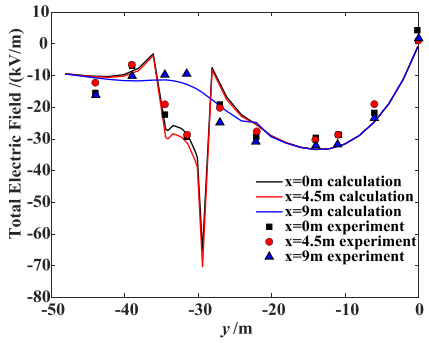

FIGURE 4. Verification of proposed method under the full-scale UHVDC test line near a full-scale residence.

TABLE 1. Geometrical parameters of a cubic building case.

Parameters	Values
Sub-conductor diameter r_0 (mm)	42.1
Bundle number	6
Bundle spacing BS (cm)	50
Line height H (m)	22
Conductor separation PD (m)	19
Building width W_1 (m)	10
Building length L_1 (m)	20
Building height H_1 (m)	8
Distance from line center to building LBD (m)	65

Jinshang-Hubei ±800 kV UHVDC Transmission Project. In these cases, TEFs on residences of cubic shape, L-shaped and a typical complex shape adjacent to this line are calculated to demonstrate the ability of the proposed method in coping with buildings of complicated geometry, which is presently not offered by other methods. Note these three shapes are frequently encountered during field investigations and are therefore representative. The maximum TEFs are also compared with the limit value 25 kV/m prescribed by the newly-issued Chinese National Standard GB39220-2020 [1].

A. CUBIC BUILDING

To show the existence of cubic buildings adjacent to lines in practice, a picture of a cubic building in the vicinity of the Jinshang-Hubei line is displayed in Figure 5(a). Its geometric hyperfine structure is omitted and it is modeled as an ideal cube. The geometrical parameters are showcased in Figure 5(b) and their corresponding values are listed in Table 1. It is important to note that the parameters in the table are similar to those in practice. The calculated TEF on the top surface of the cubic residence is shown in Figure 5(c). It can be observed that TEF on the top surface of the residence has a concave shape, being high near the edge and low at the center. The maximum TEF is close to 14 kV/m which is less than the limit value 25 kV/m. Therefore, no measure has to be taken to control the TEF in this case. The minimum TEF is roughly 6.2 kV/m, and the ratio of the maximum to minimum TEFs is approximately 2.

B. L-SHAPED BUILDING

To show the existence of L-shaped building in practice, a picture of this type is presented in Figure 6(a).

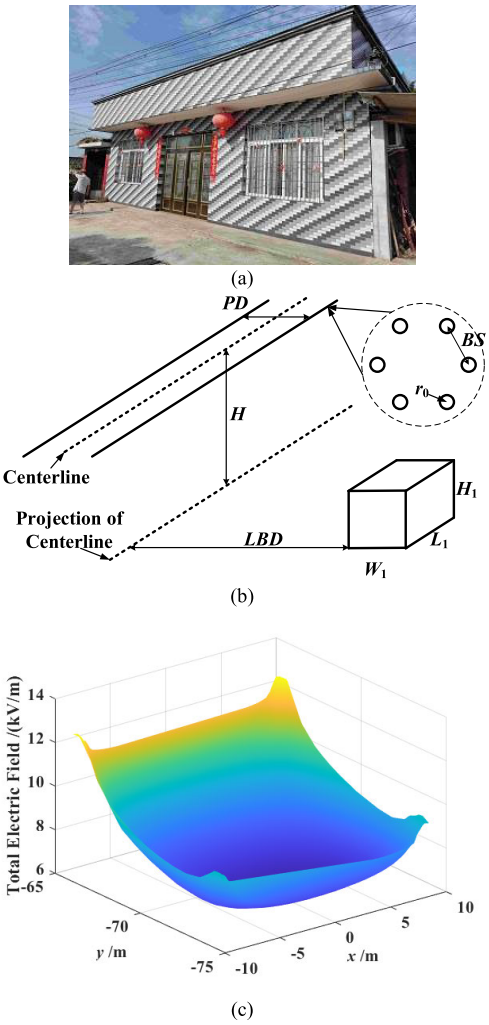

FIGURE 5. (a) The picture of a cubic building, (b) the sketch of the computation model and (c) the TEF on the top surface.

TABLE 2. Geometrical parameters of a L-shaped building case.

Parameters	Values
Sub-conductor diameter r_0 (mm)	42.1
Bundle number	6
Bundle spacing BS (cm)	50
Line height H (m)	22
Conductor separation PD (m)	19
Distance from line center to building LBD (m)	65
Lower cube width W_1 (m)	10
Lower cube length L_1 (m)	20
Lower cube height H_1 (m)	8
Upper cube width W_2 (m)	5
Upper cube length L_2 (m)	20
Upper cube height H_2 (m)	4

Its geometric hyperfine structure is omitted and it is modeled as a combination of two cubes. By hyperfine structure, it means structures such as fine decorations, eaves, and the like. The geometrical parameters are displayed in Figure 6(b) and their values are listed in Table 2. The calculated TEF on the top surface of the L-shaped residence is shown in Figure 6(c). It can be seen that the TEF on the top surface of the upper cube has a slightly concave shape, being a little high near the edge and relatively low at the center, and the TEF on

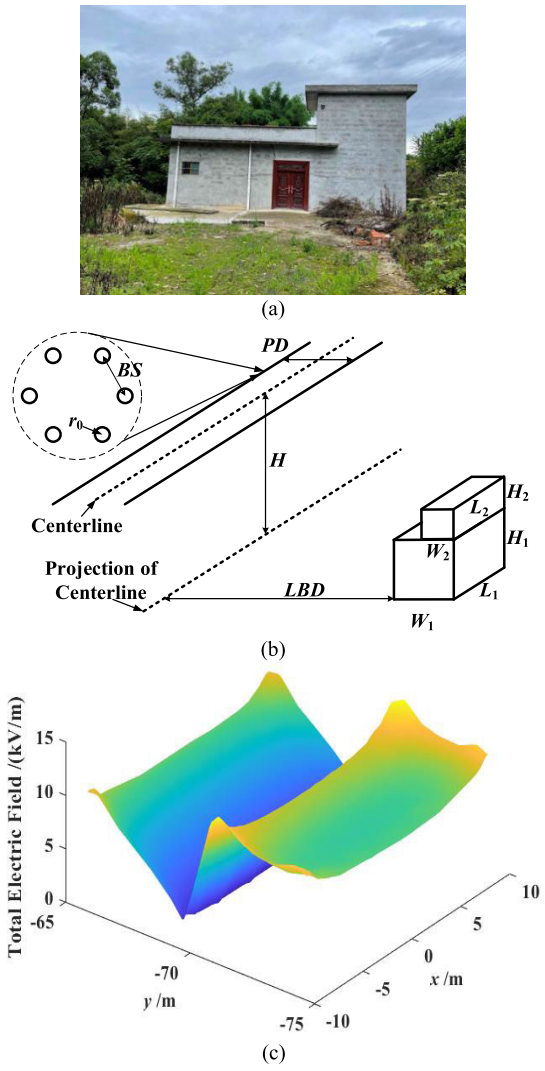

FIGURE 6. (a) The picture of a L-shaped building, (b) the sketch of the computation model and (c) the TEF on the top surface.

the top surface of the lower cube has an inclined plane shape, being high at the edge close to the transmission line and low near the wall. This is mainly due to the electrostatic shield of the wall, which declines the space-charge-free electric field and accordingly the TEF. The maximum and minimum values of the TEFs on the top of the upper cube are 13.1 kV/m and 7.9 kV/m, respectively which are higher than those in the Case A. The ratio of the maximum to minimum values is 1.7. This is understandable because the top surface of the L-shaped residence's upper cube is higher than the lower cube. The maximum and minimum values of the TEFs on the top of the lower cube are 10.7 kV/m and 1.2 kV/m, respectively, which are lower than those in the Case A. This is understandable since the TEF on the top surface of the lower cube of the L-shaped residence is weakened by the electrostatic shielding effect of the upper cube. The maximum TEF is close to 15 kV/m which is higher than that in the Case A. This is understandable since the top surface of the upper cube is higher than that of lower cube. But it is still less than

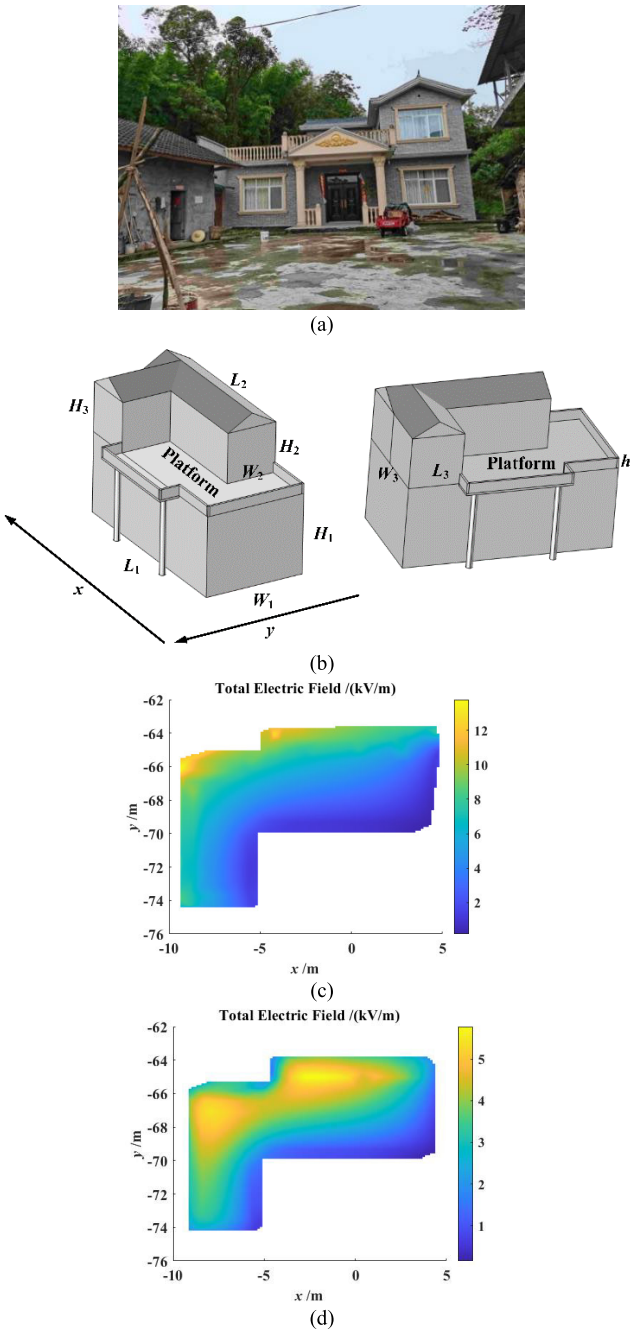

FIGURE 7. (a) The picture of a typical complex shaped building, (b) the sketch of the building model, (c) the TEF on the platform without parapet walls and (d) the TEF on the platform with parapet walls.

the limit value 25 kV/m. Therefore, no measure has to be taken to control the TEF in this case.

C. A TYPICAL COMPLEX SHAPED BUILDING

To demonstrate the capability of the proposed method in handling more complicated cases, the TEF of a residence of complex geometry was computed. The picture of this residence is presented in Figure 7(a). Its geometric hyperfine structure is omitted and it is modeled as a combination of three cubes and two prisms. Hyperfine structure refers to

TABLE 3. Geometrical parameters of a typical complex shaped building case.

Parameters	Values
Sub-conductor diameter r_0 (mm)	42.1
Bundle number	6
Bundle spacing BS (cm)	50
Line height H (m)	22
Conductor separation PD (m)	19
Distance from line center to building LBD (m)	65
Lower cube width W_1 (m)	10
Lower cube length L_1 (m)	20
Lower cube height H_1 (m)	8
Upper cube 1 width W_2 (m)	5
Upper cube 1 length L_2 (m)	15
Upper cube 1 height H_2 (m)	5
Upper cube 2 width W_3 (m)	5
Upper cube 2 length L_3 (m)	5
Upper cube 2 height H_3 (m)	5
Height of parapet wall h (m)	1

structures such as fine decorations, eaves, and the like. The geometrical parameters are displayed in Figure 7(b) and their values are listed in Table 3. It should be noted the building model contains parapet walls which are neglected previously. The calculated TEF on the platform of the residence where people constantly conduct activities is shown in Figure 7(c) and (d). It can be seen from Figure 7(c) where parapet walls are absent that the TEF near the edge face to face with the transmission line is high and declines as it goes away from the line, and the TEF decreases further as it reaches to the building walls. The maximum TEF is almost 14 kV/m. With the presence of parapet walls, the maximum TEF declines by 58 % and is down to 5.8 kV/m which is far below the limit value 25 kV/m, and the area where high TEF locates moves away from the parapet walls, as shown in Figure 7(d). This indicates parapet walls are able to weaken TEF on the platform, which is understandable because walls have an electrostatic shield effect.

VI. CONCLUSION

In this paper, a line-area element hybrid boundary element method (BEM) is proposed and introduced into FTM to calculate 3D TEF on buildings adjacent to HVDC transmission lines. FTM combined with this BEM is able to handle bundle conductors and residences of complex geometry. The method is verified by experiments and demonstrated to be applicable to cases where all previous methods have not been reported to be able to deal with residences of complex geometry so far. The ratio of the maximum to minimum TEFs on the top surface of the residences is about 2. The results also show parapet walls are conducive to leveling down TEF on residences. In the case presented in this paper, the TEF is reduced by about 58 %. Future work will be directed toward (1) speeding up the proposed line-area element hybrid boundary element method and FTM to cope with fast evaluation of TEF on large number of residences near HVDC transmission lines; (2) exploring the impact of weather; (3) conducting experiments on TEF on residences of multiple shapes

REFERENCES

[1] *Limits and Monitoring Methods of Total Electric Field of DC Transmission Project*, Standard GB39220-2020, Ministry of Ecology and Environment, Beijing, China, 2020.

[2] X. Ma, L. Xie, K. He, and J. Lu, "Research on 3-D total electric field of crossing high voltage direct current transmission lines based on upstream finite element method," *High Voltage*, vol. 6, no. 1, pp. 160–170, Feb. 2021.

[3] Y. Z. Zhen, X. Cui, Z. N. Luo, T. B. Lu, J. Y. Lu, and Y. Yang, "Finite element method for calculating total electric field of HVDC lines with underneath building," *Proc. CSEE*, vol. 31, no. 9, pp. 120–125, 2011.

[4] Y. Zhen, X. Cui, T. Lu, X. Li, C. Fang, and X. Zhou, "3-D finite-element method for calculating the ionized electric field and the ion current of the human body model under the UHVDC lines," *IEEE Trans. Power Del.*, vol. 28, no. 2, pp. 965–971, Apr. 2013.

[5] D. Wang, T. Lu, X. Cui, L. Xie, L. Zhao, Y. Ju, and J. Lu, "Electric field calculation on residential houses near UHVDC lines using 3D reconstruction method," *CSEE J. Power Energy Syst.*, vol. 5, no. 4, pp. 524–532, May 2019.

[6] Z. N. Luo, X. Cui, Y. Z. Zhen, J. Y. Lu, H. Han, and Y. Q. Liu, "Calculation method for the ionized field under HVDC transmission lines with building nearby," *Proc. CSEE*, vol. 30, no. 15, pp. 125–130, 2010.

[7] Z. Luo, X. Cui, W. Zhang, and J. Lu, "Calculation of the 3-D ionized field under HVDC transmission lines," *IEEE Trans. Magn.*, vol. 47, no. 5, pp. 1406–1409, May 2011.

[8] F. N. Xiao, B. Zhang, J. Mo, and J. L. He, "Calculation of 3-D ion-flow field at the crossing of HVdc transmission lines by method of characteristics," *IEEE Trans. Power Del.*, vol. 33, no. 4, pp. 1611–1619, Aug. 2018.

[9] F. Xiao, B. Zhang, and Z. Liu, "Calculation of ion flow field around metal building in the vicinity of bipolar HVDC transmission lines by method of characteristics," *IEEE Trans. Power Del.*, vol. 35, no. 2, pp. 684–690, Apr. 2020.

[10] J. Qiao, J. Zou, J. Yuan, J. B. Lee, and M. Ju, "Calculation of ion-flow field of HVdc transmission lines in the presence of wind using finite element-finite difference combined method with domain decomposition," *IEEE Trans. Magn.*, vol. 52, no. 3, pp. 1–4, Mar. 2016.

[11] P. Liu and V. Dinavahi, "Finite-difference relaxation for parallel computation of ionized field of HVDC lines," *IEEE Trans. Power Del.*, vol. 33, no. 1, pp. 119–129, Feb. 2018.

[12] M. A. Abouelatta, S. A. Ward, A. M. Sayed, K. Mahmoud, M. Lehtonen, and M. M. F. Darwish, "Fast corona discharge assessment using FDM integrated with full multigrid method in HVDC transmission lines considering wind impact," *IEEE Access*, vol. 8, pp. 225872–225883, 2020.

[13] M. A. Abouelatta, S. A. Ward, A. M. Sayed, K. Mahmoud, M. Lehtonen, and M. M. F. Darwish, "Measurement and assessment of corona current density for HVDC bundle conductors by FDM integrated with full multigrid technique," *Electr. Power Syst. Res.*, vol. 199, Oct. 2021, Art. no. 107370.

[14] A. M. Sayed, M. A. Abouelatta, M. Badawi, K. Mahmoud, M. Lehtonen, and M. M. F. Darwish, "Novel accurate modeling of dust loaded wire-duct precipitators using FDM-FMG method on one fine computational domains," *Electr. Power Syst. Res.*, vol. 203, Feb. 2022, Art. no. 107634.

[15] A. S. Zalhaf, D.-E.-A. Mansour, Y. Han, P. Yang, and M. M. F. Darwish, "Numerical and experimental analysis of the transient behavior of wind turbines when two blades are simultaneously struck by lightning," *IEEE Trans. Instrum. Meas.*, vol. 71, 2022, Art. no. 9001612.

[16] S. P. Maruvada, *Corona Performance of High-Voltage Transmission Lines*. Baldock, U.K.: Research Studies Press, 2000, pp. 192–193.